

Estimation of the masses in the Local Group by Gradient Boosted Decision Trees

Edoardo Carlesi ¹ ^{*}, Yehuda Hoffman ¹ [†], Noam I Libeskind ^{2,3}

¹*Racah Institute of Physics, Hebrew University, Jerusalem, Israel*

²*Leibniz Institut für Astrophysik Potsdam (AIP), An der Sternwarte, Potsdam, Germany*

³*University of Lyon, UCB Lyon 1, CNRS/IN2P3, IUF, IP2I Lyon, France*

Submitted XXXX XXX XXXX

ABSTRACT

Our goal is to estimate the mass of the Local Group (LG) and the individual masses of its primary galaxies, the M31 and the Milky Way (MW). We do this by means of a supervised machine learning algorithm, the gradient boosted decision trees (GBDT) and using the observed distance and relative velocity of the two as input parameters. The GBDT is applied to a sample of 2148 mock LGs drawn from a set of 5 dark matter (DM)-only simulations, ran withing the standard Λ CDM cosmological model. The selection of the mock LGs is guided by a LG model, which defines such objects. The role of the observational uncertainties of the input parameters is gauged by applying the model to an ensemble of mock LGs pairs whose observables are these input parameters perturbed by their corresponding observational errors. Finally the observational data of the actual LG is used to infer its relevant masses. Our main results are the sum and the individual masses of the MW and M31: $M_{tot} = 3.31^{+0.79}_{-0.67}$, $M_{MW} = 1.15^{+0.25}_{-0.22}$ and $M_{M31} = 2.01^{+0.65}_{-0.39} \times 10^{12} M_{\odot}$ (corresponding to the median and the 1st and 3rd quartiles). The ratio of the masses is $M_{M31}/M_{MW} = 1.75^{+0.54}_{-0.28}$, where by convention the M31 is defined here to be the more massive of the two halos.

Key words: Cosmology, Numerical simulations, Dark matter, Local Group

1 INTRODUCTION

In recent years, a substantial development in cosmology has been driven by the increase in quality and quantity of observational data in the nearby Universe. In fact, thanks to the sharp improvement in cosmological simulations, it has been possible to test to higher degrees of accuracy, the predictions of the standard Λ Cold Dark Matter (Λ CDM) model on small scales. In particular, observations of the Local Group (LG) of galaxies has shaped galaxy formation theories and their links to cosmology at large (Boylan-Kolchin et al. 2012; Zavala et al. 2012; Tollerud et al. 2014; Elahi et al. 2015; Penzo et al. 2016; Garaldi et al. 2016; Carlesi et al. 2017). However, the estimation of the masses of the LG as well as its two main constituents - the Milky Way (MW) and Andromeda (M31) galaxies - is still an open unresolved issue.

The so-called *timing argument* model (Kahn & Woltjer 1959; Lynden-Bell 1981), even with the simplifying assump-

tions of a purely radial orbits and a first time infall for the MW and M31, provides a good proxy to the dynamics of the LG. It applies the Newtonian two-body problem model to integrate the equations of motion of the LG from the Big Bang to the present epoch. This approach can be extended by including the Large Magellanic Clouds (Peñarrubia et al. 2016) and Dark Energy (Partridge et al. 2013). Other methods of mass estimation usually rely on cosmological simulations, e.g. in Carlesi et al. (2016) where it was highlighted the effect of the uncertainty in the transverse velocity of the MW-M31 system, in McLeod et al. (2017) who estimated the impact of the large scale structure on the mass value and the likelihood-free inference method of Lemos et al. (2021), who used *Gaia* data (Gaia Collaboration 2016) in combination with large dark matter simulations.

The *timing argument* model assumes a very simplified presentation of the LG - two point-like objects of time invariant masses and unperturbed by the rest of the universe. The mass of the LG is defined as the sum of the masses of the two bodies. The actual LG is much more complicated than that. It is made of two main extended bodies of time evolving masses as well as dozens of smaller satellite galax-

* E-mail: ecarlesi83@gmail.com

† E-mail: hoffman@huji.ac.il

ies; and its dynamics is affected by the tidal field exerted by the external universe. The notion of the ‘mass of the LG’ is not well defined and it strongly depends on how the LG is defined. We try here to stay close to the spirit of the *timing argument* model and use the sum of the masses of the MW and M31 as a proxy to the mass of the LG.

Machine learning (ML) algorithms have been shown to be extremely useful tools in cosmology and astrophysics. Given their capability of modelling non-linear relationships, they have been used to address a vast array of different issues, such as galaxy classification (Naim et al. 1995), cosmological model selection (Merten et al. 2019; Peel et al. 2019), dark matter halo properties (Lucie-Smith et al. 2018, 2019, 2020), local group mass (McLeod et al. 2017; Lemos et al. 2021), the relation between gas and dark matter distribution (Machado Poletti Valle et al. 2020), photometric redshifts (Collister & Lahav 2004) and galaxy properties in surveys (Mucesh et al. 2021), among others. In the present context ML refers to a class of computational techniques that assign output values to a set of input parameters, called in the ML jargon *features*. The unique character of ML algorithms is that they bypass the standard approach of solving analytically or more often numerically a set of non-linear equations. Instead statistical hidden relations are used to predict a desired solution. The term *supervised machine learning* refers to a wide class of ML algorithms that are trained and validated by using large datasets for which the desired output values are known - either by detailed calculations or by extra observations or measurements - for the input data.

We aim here at estimating the masses of the LG and the MW and M31 galaxies from the observed kinematics of the LG within the framework of supervised ML, applying the *gradient boosted decision trees* (GBDT) algorithm to the observed values of the distance between the MW and the M31 galaxies and their relative radial and tangential velocities to calculate the above masses. The supervised nature of the ML requires the construction of an ensemble of mock LGs, that closely emulate the actual observed LG, for which the full dynamics of such objects is available, in particular both the relative distances and velocities of the mock MW and M31 and their masses are known. A sample of mock LGs is constructed here from a set of cosmological DM-only N -body simulations. DM halos are used as proxies for the MW and M31 galaxies and the mass of the LG is approximated here by $M_{\text{tot}} = M_{\text{MW}} + M_{\text{M31}}$, while the individual masses are the corresponding halo masses. The training and validation of the GBDT to the ensemble of mock LGs yields the desired non-linear mapping from the input features to the desired masses. The simulations are conducted within the standard Λ CDM cosmological model and the mock LGs are defined by an assumed LG model (see below). We are interested here in the posterior distribution of the output masses given the observed input features and the prior distribution of their associated uncertainties and within the framework of the Λ CDM and the LG models. This is done by constructing an ensemble of Monte Carlo realizations of possible observed features and using the GBDT algorithm to map it into an ensemble of possible outcomes. This is used to estimate the mean and scatter of the predicted masses.

The paper is structured as follows. §2 presents the LG model. The construction of the ensemble of mock LGs, that are used as the training and validation sets, is summarized

in §3. Only a brief introduction to the vast issue of supervised ML, in general, and the GBDT methodology is given here (§4). The application of the GBDT algorithm to the actual LG is presented in §5. A summary and general discussion conclude the paper (§6).

2 THE LOCAL GROUP MODEL

A selection of mock LGs from simulations needs to be preceded by a discussion of what defines it in simulations. Namely, one needs to outline the rules that capture the main relevant properties of the observed LG and use it for selecting mock LGs from the simulations. This is the so-called Local Group Model (see Carlesi et al. 2016). In the context of the dynamical modeling of the LG the model focuses on the following properties of the two main DM halos that constitute the LG: masses, mass ratio, isolation, separation and relative velocity. In this case, the parameters and their allowed intervals are: 1. Halo masses: (M_{200} , that is the total mass enclosed within the radius at which the density is 200 times the critical one) within $(0.5 - 4.0) \times 10^{12} h^{-1} M_{\odot}$; 2. Mass ratio: $M_{\text{M31}} : M_{\text{MW}} < 4$; 3. Separation: $r = (0.4 - 1.3) h^{-1} \text{Mpc}$; 4. Isolation, i.e. no other halo of mass $\geq M_{\text{MW}}$ within $2h^{-1} \text{Mpc}$; 5. Radial velocity: $v_{\text{rad}} < 0 \text{ km s}^{-1}$. A further assumption is made that the M31 galaxy is the more massive member of the LG. This choice does not affect the outcome of the analysis and is made for the sake of mathematical convenience and as a way of labelling the most massive halo of the LG. Yet, it is motivated by Karachentsev et al. (2009) and Diaz et al. (2014), though a more massive Milky Way cannot be excluded (Gottesman et al. 2002; Ibata et al. 2004).

The results presented here are valid under the assumption of Λ CDM and the LG models. In a Bayesian language these models serve as the prior which conditions the results that follow.

A general comment concerning the h^{-1} scaling is due here, where $h = H_0/100 \text{ km s}^{-1} \text{Mpc}^{-1}$ and H_0 is Hubble’s constant. As far as data drawn from simulations is concerned, such as masses and distances, the h^{-1} is used. Data from observations of the actual LG appears without that scaling.

3 THE TRAINING AND VALIDATION DATASETS

Supervised ML algorithms are based on the availability of a given set of data for which the sought after results are known. In the astrophysical context where the LG is a unique object one needs to resort to selecting mock LGs from simulations, for which all the information - including the masses of the MW- and M31-like halos - is known. The training and validation datasets are taken here from a set of five DM only N -body simulations (introduced in Carlesi et al. 2019) with 1024^3 particles within a $100 h^{-1} \text{Mpc}$ box with Planck-I cosmological parameters (Planck Collaboration 2014). The halo catalogs were obtained with AHF (Knollmann & Knebe 2009), which uses an adaptive mesh refinement technique to identify halo centers as density peaks in the matter field and iteratively removes gravitationally unbound particles. The mass of a halo extracted from the nu-

merical simulations is defined by M_{200} , namely the mass inside a sphere within which the mean density is 200 times the critical density, an attribute of the AHF halo finder (Knollmann & Knebe 2009, for details).

The LG model provides a very generous definition of the LG that allows to build up a robust sample of 2148 objects to be used for the training and validation of the ML algorithm. As mentioned above, the LG model does not distinguish between the MW and M31 halos and therefore we somewhat arbitrarily follow the commonly held convention that $M_{MW} < M_{M31}$. The median and the 1st and 3rd quartiles of the distribution of the mock LGs are: $M_{MW} = 0.64_{-0.17}^{+0.41} \times 10^{12} h^{-1} M_{\odot}$ and $M_{M31} = 1.39_{-0.54}^{+0.94} \times 10^{12} h^{-1} M_{\odot}$. The mock LGs are designed to emulate the dynamics of the observed LG. As such the data that defines a mock LG consists of the distance (r) between the two main halos of the object and their relative radial and tangential velocities (v_{rad} and v_{tan}). These are defined with respect to the center of mass of the halos.

4 SUPERVISED MACHINE LEARNING

4.1 Basics

The problem addressed here is of an estimation of M_{tot} , M_{MW} , M_{M31} and M_{MW}/M_{M31} given three input parameters that define a LG by means of supervised ML. Our approach adopted is to calculate the four output parameters (results) independently of one another. Namely four independent ML functionals are constructed as follows:

$$\begin{aligned} M_{MW} &= D_{MW}(r, v_{rad}, v_{tan}) \\ M_{M31} &= D_{M31}(r, v_{rad}, v_{tan}) \\ M_{tot} &= D_{tot}(r, v_{rad}, v_{tan}) \\ r_M \equiv \frac{M_{MW}}{M_{M31}} &= D_{r_M}(r, v_{rad}, v_{tan}) \end{aligned} \quad (1)$$

The four operators D_y (where y stands for the individual masses, total mass and for the mass ratio) are multi-parameters non-linear operators that map from the three input parameters to one output parameter. The structure of these functionals is determined by the rules of the specific assumed ML algorithm and its many free parameters are determined by non-linear regression performed on a training dataset and tested against a validation dataset. This is the essence of supervised ML algorithm. The non-linear regression is performed independently for each one of the functionals of Eqs. 1.

The supervised ML algorithm used here is the GBDT that operates on a combined set of decision trees models. A brief description of decision trees models in general and of the particular GBDT method follows.

4.2 Decision Trees

A decision tree $d(\mathbf{x})$ is a supervised learning algorithm that predicts a continuous or discrete single target variable y from an array of N input features $\mathbf{x} = (x_0, \dots, x_{N-1})$ which describes each data point. In the particular case considered here we have $N = 3$. The input features are processed through a set of nodes - Boolean conditions with a 'yes' or 'no' outcome - and ends up with one possible outcome

out of predetermined possible outcomes. In the language of decision trees methods the possible outcomes are denoted as leaves. In the case where the physical nature of the outcome y is that of a continuous variable the number of leaves dictates the numerical resolution of the tree. For a discrete target variable y , e.g. in a classification problem, the number of leaves equals the number of possible classes. A given decision tree is defined by the number and arrangements of the nodes and leaves - these are considered the hyper-parameters of the particular tree. A given node consists of the Boolean condition of whether $x_n > c_i$, where $n = 0, \dots, N-1$ and $i = 0, \dots, I-1$ with I being a hyper-parameter that determines the number of thresholds c_i . The decision tree shown in Fig. 1 is designed for $N = 3$ features, $I = 6$ nodes and $N_{leaf} = 7$ leaves. Such a decision tree can assign one out of 8 possible pre-determined numerical values for the questioned asked, namely \hat{y} accepts one of the possible values of y_l ($l = 0, \dots, N_{leaf} - 1$). Here, an estimate of the total mass of the LG, say, is $\hat{y} = d_{LG}(r, v_{rad}, v_{tan})$.

The optimization of a given tree proceeds as follows. The hyper-parameters within which the optimization is done are the maximum depth of the tree (n_{depth}) and the maximum number of leaves (N_{leaf}), which are selected ab initio. The structure of the nodes, ensemble of parameters $\{c_i\}$, their number I and the actual number of leaves N_{leaf} are fixed by the optimization, which is done by the minimization the loss function L defined as the mean 'distance' between the actual and the predicted value taken over all members of the training set,

$$L = \frac{1}{N_{train}} \left(\sum_0^{N_{train}} (y_{\alpha} - \hat{y}_{\alpha})^2 \right)^{1/2}, \quad (2)$$

where N_{train} is the number of data points in the training set and the sum extends over all all members of that set.

4.3 Gradient boosted decision trees

Decision trees are often considered to be 'weak learners' - their simple structure tends to keep their predicted output 'close' to the data of the training set, hence they are prone to over-fitting. Further boosting is needed to overcome it. The gradient boosted decision trees algorithm (Freund & Schapire 1997; Friedman 2001) is an ensemble method where several decision trees are combined together to provide a more reliable estimate of the target output.

In the the random forest algorithm an ensemble of N_{tree} decision trees, all having the same hyper-parameters, is constructed. The number of the trees and their hyper-parameters are fixed at the onset of the calculation. The random forest estimator is the ensemble averaged value of the output of the individual trees defined by:

$$D(x) = \frac{1}{N_{tree}} \sum_{j=1}^{N_{tree}} d_j(x). \quad (3)$$

An alternative approach is to start with one tree $d_1(x)$ and gradually add successively more trees, $d_2(x), d_3(x), \dots, d_i(x)$, again all constructed with the same hyper-parameters. Given the first i decision trees, a new es-

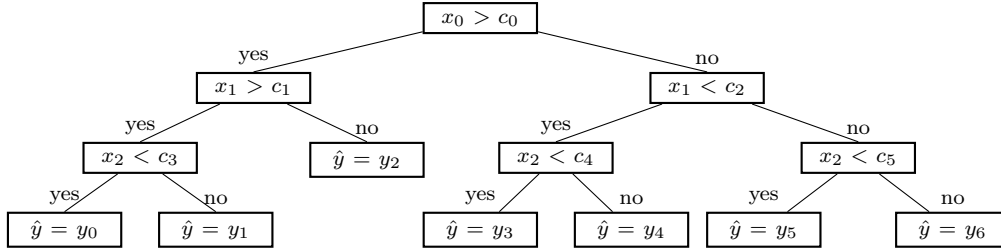


Figure 1. A graphic presentation of a schematic example of a decision tree defined by $N = 3$ input features, x_0, \dots, x_{N-1} , $I = 6$ nodes and $N_{leaf} = 7$ leaves. The x_n is the n -th component of a given data point, c_i is the i -th constant that defines the threshold value of the i -th node and y_{nl} is the nl -th leaf, namely a possible \hat{y} outcome, that the decision tree can predict.

imator $D_i(x)$ is constructed by

$$D_j(x) = \frac{1}{j} \sum_{j'=1}^j w_{j'} d_{j'}(x), \quad (4)$$

whose output is $\hat{y}_j = D_j(x)$. The weights $w_{j'}$ and the parameters of $d_{j'}(x)$ are adjusted in order to ensure that $L_j < L_{j-1}$. The procedure is iterated until the desired number of total trees N_{tree} is reached. The hyper-parameters and the number of trees are gauged by the convergence of L_j , calculated for the training set. This is the gradient boosted decision trees algorithm, and it is the method chosen here to estimate the masses of the LG.

The essence of the GBDT algorithm is the non-linear mapping from a set of input features to an outcome, namely, a prediction, whose possible numerical values is spanned by the set of leaves. The structure of a single decision tree or the full GBDT mapping is done by a complex non-linear regression with respect to a loss function in a way that does not easily yield itself to a simple analytical understanding. Yet these algorithms can rank the input features by their importance, namely by the sensitivity of the outcome, i.e. result, to the different features. The output of a single decision tree or the GBDT algorithms is a rearrangement of the input features by a decreasing order of importance. The output is most sensitive to the first feature and the least to the last one. In a way this is akin to the order of modes in the principal component analysis (PCA; Press et al. 2002). A detailed description on how the importance ranking is done is beyond the scope of the paper. Much like in the PCA case the importance ranking provides insight to the nature of the underlying physical processes, where a low feature importance means that the desired outcome depends weakly on it. It provides also a tool for the reduction of the dimensionality of the data, and thereby increase the computational efficiency of a given case.

For the specific GBDT algorithm used here the following hyper-parameters need to be specified ab initio: the number of trees (N_{tree}), the maximum depth of the tree (N_{depth}) and the minimum number of elements per leaf node N_{min_leaf} . The later parameter refers here to the minimal number of mock LGs, drawn from the training set, so as to avoid overfitting the algorithm to the training data. Avoiding such a constraint might lead to the number of leaf nodes being equal to the number of input mock LGs. The analysis presented here has been using the Python code MLEKO¹,

Table 1. Slope c of the predicted versus true value; median μ and scatter σ for the (\hat{y}/y) computed for M_{tot} , M_{MW} , M_{M31} and r_M . The errors have been computed by a bootstrapping method to test for the robustness of the results. The deleted text has been moved to the main body of the text.

	M_{tot}	M_{MW}	M_{M31}	r_M
c	0.47 ± 0.03	0.46 ± 0.03	0.47 ± 0.03	0.38 ± 0.04
μ	0.006 ± 0.002	-0.12 ± 0.01	-0.07 ± 0.01	0.011 ± 0.005
σ	0.23 ± 0.02	0.46 ± 0.07	0.39 ± 0.03	0.15 ± 0.03

which relies on the `scikit-learn` (Pedregosa et al. 2011) implementation of the GBDT algorithm.

4.4 Training and testing

The sample of 2148 mock LGs are split into 1611 training and 537 validation sets. The GBDT hyperparameters are gauged and optimized by monitoring over the mock LGs of the training set of the slope (c) between predicted versus true values, $y_{pred} = cy_{true}$ and the the median (μ) and the standard deviation (σ) of the residual $y_{pred} - cy_{true}$. Here y stands of the \log_{10} of M_{MW} , M_{M31} and M_{LG} and of the mass ratio r_M . The resulting estimation is then then tested against the validation set.

The uncertainties in the GBDT estimated slope, median and standard deviation are obtained according to a boot strapping technique. Accordingly, 200 pairs are randomly drawn from the 537 validation data. For each draw, a value for the slope c , the median μ and standard deviation (σ) are computed. The values reported in Table 1 are the means and the standard deviations computed over these 200 subsamples.

Our main results are obtained for $n_{tree} = 250$, $n_{depth} = 10$ and $n_{leaf} = 5$. These are presented in Table 1 and in Figs. 2 and 3. Summary of these results follow: The correlation between the true and predicted value c is in the range $0.37 - 0.49$, in the case of M_{tot} this value is comparable with $c \approx 0.6$ quoted by McLeod et al. (2017) as obtained with an artificial neural network algorithm (ANN). The medians (μ) of the ratio of the log of the predicted to the true value, of M_{tot} and the mass ratio is essentially unbiased with

¹ MLEKO (Meaning milk in Serbian language) stands for Ma-

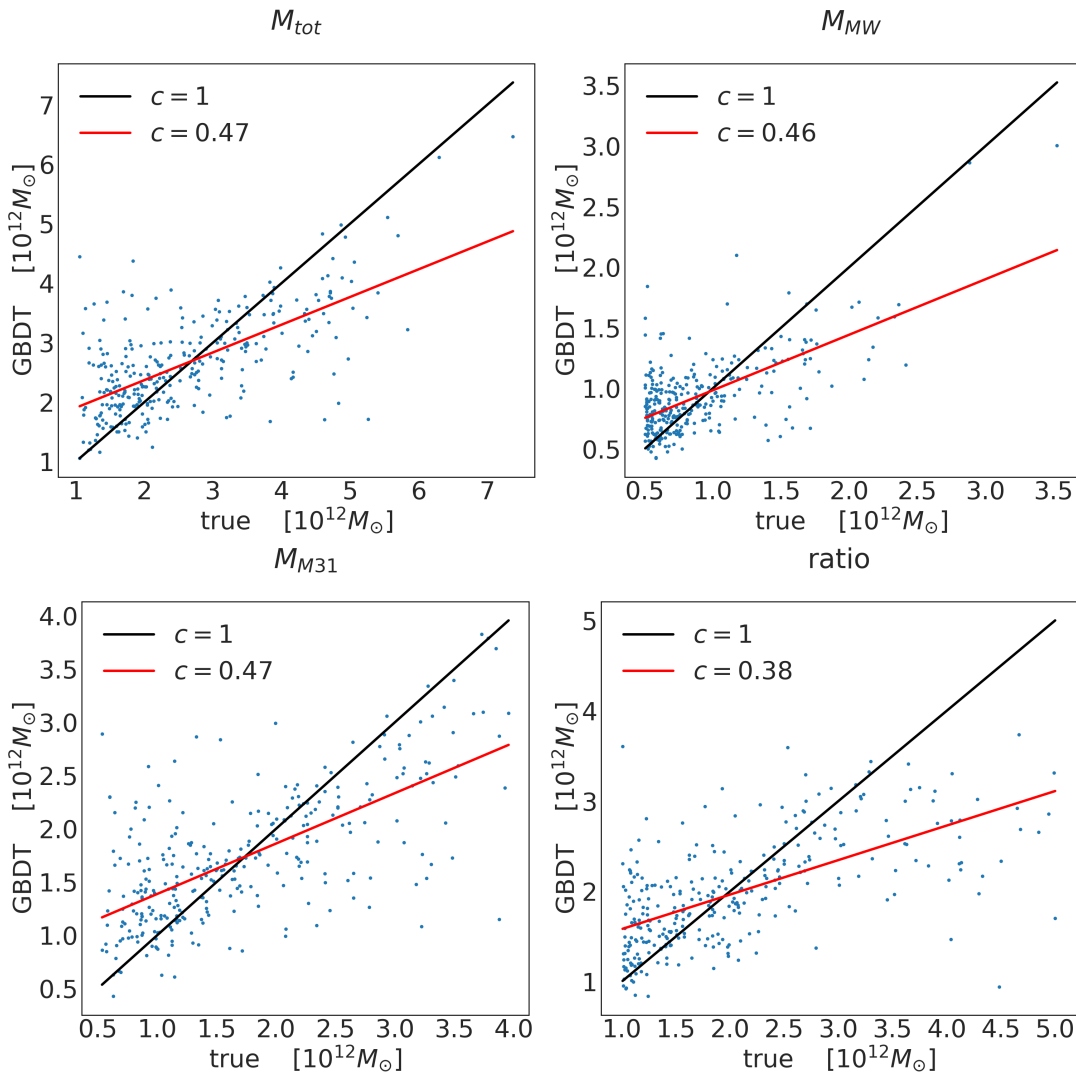


Figure 2. The GBDT algorithm applied to the mock LGs of the validation set: The M_{tot} (upper-left), M_{MW} (upper-right), M_{M31} (lower-left) and the ratio $M_{\text{M31}} / M_{\text{MW}}$ (lower-right) panels show scatter-plots of the predicted vs. the true values. The red solid line show the best fit slope (c) obtained here for the predicted vs the true values. The case of slope of unity is shown for reference (blue solid line).

a relatively small scatter. The predictions of the masses of the individual MW and M31 galaxies are less robust, yet the medians of the distribution of the log of the masses are well within the scatter. The mass of M31 is somewhat better predicted than that of the MW galaxy. The nature of the LG model assumed here readily explains these shortcomings. The masses of the individual galaxies are associated here those of the corresponding halos, identified here by AHF halo finder - a definition that relies on the virial theorem. The mass function of such halos in the mass range defined by the LG model is a strongly decreasing function of the mass. Given the fixed range of masses associated with the MW and M31 galaxies, one expects the GBDT to somewhat underestimate the masses of the individual galaxies, and that of the MW, which by definition is the less massive one, to be more affected by that bias. It can be removed by properly revising the LG model, but this lies beyond the scope of the paper.

Table 2. Mean and standard deviation values for r , v_{rad} , and v_{tan} used to generate the MC data sample.

	μ	σ	unit
r	770	40	kpc
v_{tan}	57	35	km s^{-1}
v_{rad}	105	5	km s^{-1}

5 APPLICATION TO THE ACTUAL LOCAL GROUP

5.1 Monte Carlo sampling of errors

The input parameters of the GBDT algorithm are the following observables: the distance (r), relative radial and (v_{rad}) and tangential (v_{tan}) velocities of the MW and M31 galaxies. Observational estimates of these observables and their observational uncertainties are presented in Table 2. The es-

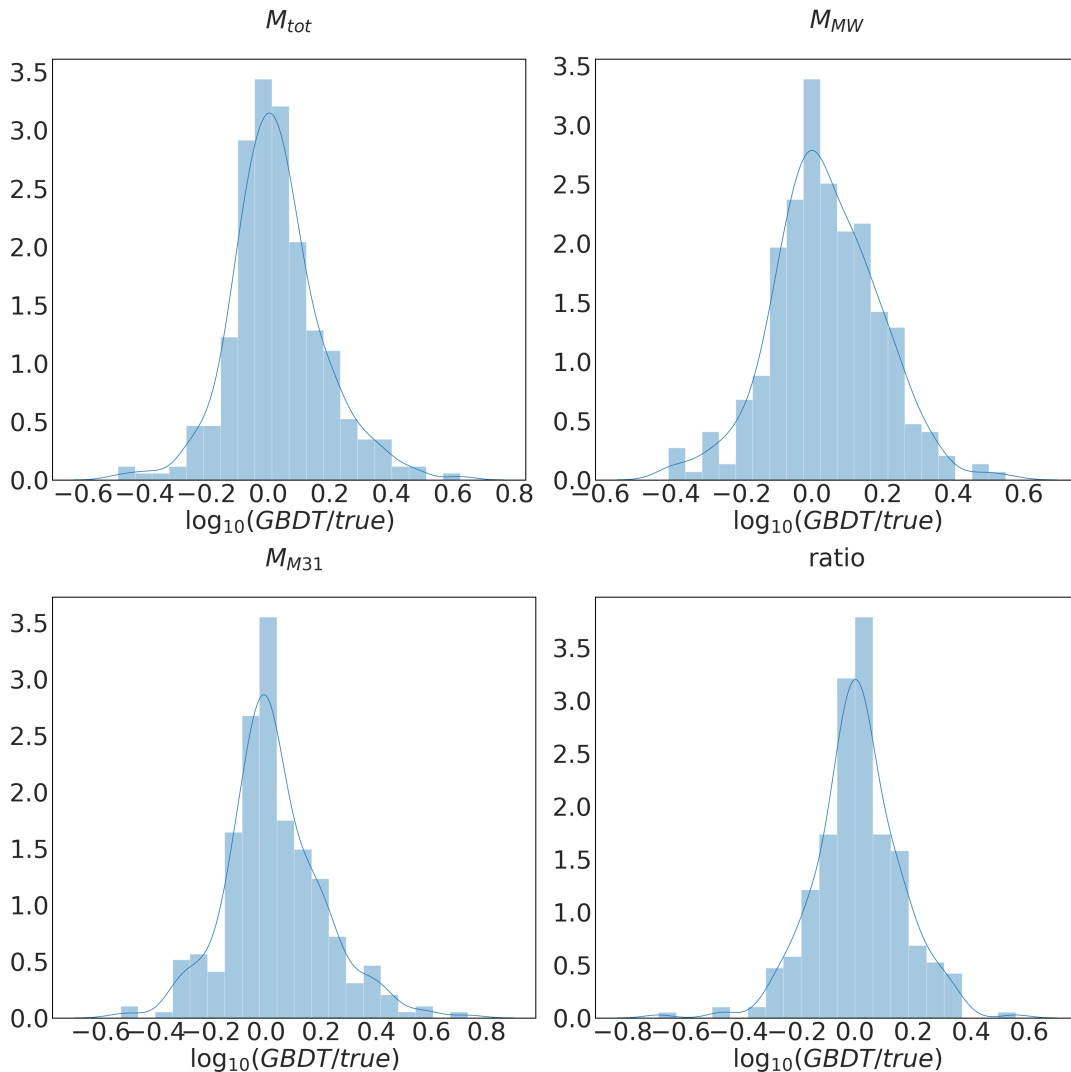


Figure 3. The GBDT algorithm applied to the mock LGs of the validation set: The M_{tot} (upper-left), M_{MW} (upper-right), M_{M31} (lower-left) and the ratio $M_{\text{M31}} / M_{\text{MW}}$ (lower-right) panels show the histogram of the \log_{10} of the ratios of the predicted over the true masses and of the predicted over the true values of r_M . The solid lines on the histograms are the smoothed kernel density estimates of the distributions.

timations of the distances and radial velocity are taken from van der Marel et al. (2012) and of the tangential velocity from van der Marel et al. (2019) (using *Gaia* data).

The uncertainties in the inferred GBDT masses and their ratio are estimated by means of the forward modeling. Namely, given the data of Table 2 an ensemble of 10^4 Monte Carlo realizations of the possible values of input parameters of the actual LG has been generated. The realizations are generated by assuming normal distribution of the uncertainties, and are done under the assumption of uncorrelated errors. The GBDT is then applied to that ensemble of possible values of input parameters. The key assumption that is made here is that the uncertainties quoted in Table 2 are statistically uncorrelated.

5.2 Results

The ensemble of 10^4 Monte Carlo realizations of the possible values of the LG (M_{tot}), the Milky Way (M_{MW}), and the M31 (M_{M31}) and the ratio of the masses of the two galaxies r_M is used to calculate the posterior distribution of these masses and ratio of the masses. The posterior distribution functions - given the observables, the LG model and the Λ CDM model - are presented in Figs. 4 and 5. The medians and the lower and upper quartiles are given in Table 4. The main results of the GBDT analysis are presented here. No attempt is made here to convert all the masses quoted in Table 4 to a unified definition. The halo mass, taken from the analysis of numerical simulations, used here and also by McLeod et al. (2017) and Lemos et al. (2021) is M_{200} as defined by the AHF halo finder.

Feature importance: A unique feature of the the GBDT algorithm is its ability to rank features, i.e. the input parameters, by their importance. Namely the weight each feature

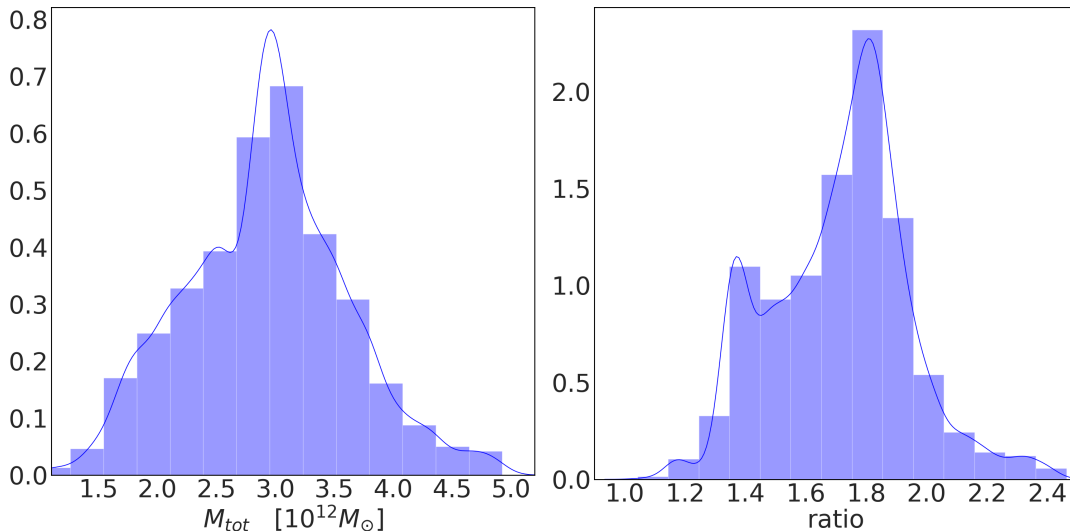


Figure 4. GBDT estimate of the total mass (left panel; note the linear scale of the mass) and of the ratio of M_{M31}/M_{MW} (right panel). The histogram correspond to the distribution of the Monte Carlo realizations of the observational uncertainties. Smoothed kernel density estimates are plotted on top with solid lines.

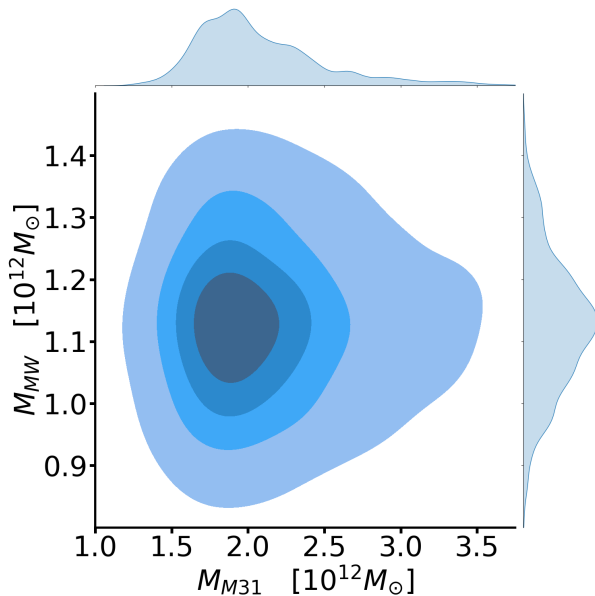


Figure 5. Joint smoothed kernel density estimate for the GBDT estimate of MW and M31 masses obtained with mock Monte Carlo realizations of the observational uncertainties. The univariate smoothed estimates are also projected.

carries in producing the final output value is estimated. Our first result is that the three features have the same weight ≈ 0.33 (Table 3), and therefore are equally important for the determination of the various masses and the mass ratio reported here. This is consistent with the results of Carlesi et al. (2017), which explored the impact of the different LG models on mass predictions, finding that modification in the priors for v_{tan} , v_{rad} and r lead to comparable changes in the results.

Table 3. Feature importance for the four GBDT models.

	r	v_{rad}	v_{tan}
M_{tot}	0.33	0.35	0.32
M_{MW}	0.35	0.33	0.32
M_{M31}	0.34	0.35	0.31
r_M	0.33	0.34	0.34

Total mass: The GBDT estimate of $M_{\text{tot}} = 3.31^{+0.79}_{-0.67}$ (all masses are in $10^{12}M_{\odot}$ units) is in a very good agreement with the results of van der Marel et al. (2012) and McLeod et al. (2017), while it lies between the smaller results of Peñarrubia et al. (2016) and Diaz et al. (2014) and the higher ones by González et al. (2014); Fattahi et al. (2016) and Lemos et al. (2021) (see the first block of Table 4)

Milky way mass: The GBDT estimation of $M_{\text{MW}} = 1.15^{+0.25}_{-0.22}$ is in a very good agreement with the *Gaia* value of (Watkins et al. 2019) as well as earlier estimates by Battaglia et al. (2005); McMillan (2011); González et al. (2014); McMillan (2016) within the same mass range. The present estimate is halfway between the results of e.g. Gibbons et al. (2014); Carlesi et al. (2016) and the ones above predicted from the analysis of high velocity stars of (Fragione & Loeb 2017) or the value of implied by a bound orbit for Leo I (Boylan-Kolchin et al. 2013), reported in the second block of Table 4.

M31 mass: The GBDT estimation of $M_{\text{M31}} = 2.01^{+0.65}_{-0.39}$ is in good agreement with the results obtained by Fardal et al. (2013), and Diaz et al. (2014) as well as the results of Carlesi et al. (2017) obtained for a non radial motion (i.e. high v_{tan}) of M31 with respect to MW (see Table 4).

Mass ratio: The GBDT model estimate of $r_M = 1.75^{+0.54}_{-0.28}$ is in agreement with that of Baiesi Pillastrini (2009),

Table 4. Comparison between the GBDT results and some of the other methods found in the literature to estimate M_{tot} , M_{MW} , M_{M31} and the mass ratio of M31 to MW. We can see that the GBDT method provides estimates that compare favourably with previous results and make it suitable for a wide range of different applications.

Reference	$M_{\text{tot}}[10^{12}M_{\odot}]$
Present paper	$3.31^{+0.53}_{-0.45}$
van der Marel et al. (2012)	3.17 ± 0.57
González et al. (2014)	$4.17^{+1.45}_{-0.93}$
Peñarrubia et al. (2016)	$2.64^{+0.42}_{-0.38}$
Carlesi et al. (2016)	$3.47^{+1.16}_{-0.83}$
McLeod et al. (2017)	$3.6^{+1.3}_{-1.1}$
Lemos et al. (2021)	$4.6^{+2.3}_{-1.8}$

Reference	$M_{\text{MW}}[10^{12}M_{\odot}]$
Present paper	$1.15^{+0.25}_{-0.22}$
Battaglia et al. (2005)	1.2 ± 0.5
McMillan (2011)	1.26 ± 0.24
Boylan-Kolchin et al. (2013)	$1.6^{+0.8}_{-0.6}$
González et al. (2014)	$1.14^{+1.19}_{-0.41}$
Diaz et al. (2014)	0.8 ± 0.5
McMillan (2016)	1.3 ± 0.3
Carlesi et al. (2016)	$0.82^{+0.33}_{-0.38}$
Fragione & Loeb (2017)	$1.2 - 1.7$
Watkins et al. (2019)	$1.28^{+0.97}_{-0.48}$

Reference	$M_{\text{M31}}[10^{12}M_{\odot}]$
Present paper	$2.01^{+0.65}_{-0.39}$
Fardal et al. (2013)	$1.99^{+0.51}_{-0.41}$
Diaz et al. (2014)	1.7 ± 0.3
Carlesi et al. (2016)	$2.48^{+0.80}_{-0.56}$
Peñarrubia et al. (2016)	$1.33^{+0.97}_{-0.48}$

Reference	$M_{\text{M31}}/M_{\text{MW}}$
Present paper	$1.75^{+0.54}_{-0.28}$
Baiesi Pillastrini (2009)	2.5 ± 0.5
Diaz et al. (2014)	$2.3^{+2.1}_{-1.1}$

estimated studying the tidal perturbations of M31 to the LG and Diaz et al. (2014) obtained by balancing the angular momentum at the LG center of mass, as can be seen in the last block of Table 4.

6 DISCUSSION

A supervised machine learning algorithm, the gradient boosted decision trees, is derived so as to estimate the masses of the Local Group and its main components, the Milky Way and M31 galaxies, and their mass ratio, from the observed distance and relative velocity of the two. The algorithm is trained and validated against a sample of 2148 mock LGs drawn from a set of five DM only N -body simulations (see Carlesi et al. 2019) with 1024^3 particles within a 100

h^{-1} Mpc box with Planck-I cosmological parameters (Planck Collaboration 2014). The halo catalogs were obtained with AHF halo finder (Knollmann & Knebe 2009). The selection of the mock LGs is based on a LG model introduced here.

A summary of the main results is: a. Total mass of the LG, $M_{\text{tot}} = 3.31^{+0.79}_{-0.67}$ (median and 1st and 3rd quartiles; masses are in $10^{12}M_{\odot}$ units); b. Mass of the MW galaxy, $M_{\text{MW}} = 1.15^{+0.25}_{-0.22}$; c. Mass of the M31 galaxy $M_{\text{M31}} = 2.01^{+0.65}_{-0.39}$; d. The mass ratio $M_{\text{M31}}/M_{\text{MW}} = 1.75^{+0.54}_{-0.28}$; e. Features importance of the three input parameters, distance, relative radial and tangential velocities, is roughly equal. The estimated masses of the two individual galaxies and of the total mass of the LG are in reasonable to very good agreement with other published estimates and as such we do not expect them to be controversial. Our estimate of the mass ratio stands out to some degree. The issue of possible approximate equality of the masses of the Milky Way and M31 galaxies is open and somewhat disputed. Studies based on the timing argument for example compute a total LG mass, while studies based on the kinematics of MW stars infer a halo mass via extrapolation to the virial radius. Taken at face value, independent individual measurements (or estimations) of the MW and M31 halo masses are unable to either constrain the mass ratio, nor make firm statements on which is the more massive halo. With our approach we cannot argue which galaxy is more massive but predict that their mass ratio is $1.75^{+0.54}_{-0.28}$.

Traditionally the issue of the mass of the LG as a whole or of masses of the main objects that constitute the LG, has been dealt within a dynamical framework. Much of that work has been inspired by the *timing argument* model, which simplifies the complex dynamics and mass assembly history of the LG as the classical two-body problem, thereby envisaging the MW and M31 galaxies as two point-like particles conserving their orbital energy and angular momentum and their individual initial masses. The ‘two-body problem’ model does not capture the complexity of the dynamics of the LG (as mentioned in the Introduction). This has led to a new approach, of estimating the mass of the LG by means of ML techniques applied to simulated LG-like objects (McLeod et al. 2017; McLeod & Lahav 2020; Lemos et al. 2021). These studies gave up the hope on amending the *timing argument* model by a rigorous dynamical treatment and opted for ML techniques. Yet, the input parameters extracted from the simulations have been inspired by the simple analytical model - mostly the distance and relative velocities of the MW and M31-like objects. The success of those ML studies in estimating the mass of the LG is in some sense not surprising, as they operate within the same framework as the *timing argument* model. The success of our current analysis in estimating the individual masses of the MW and M31 galaxies is surprising, as nothing in the dynamics of the two-body problem and in the definition of the LG Model hints towards a sensitivity to these individual masses. Recent developments aiming at gaining insight to the interpretability and explainability of the results of ML methods might shed more light on the problem and add to our understanding of the dynamics of the LG (e.g. Linardatos et al. 2021; Marcinkevičs & Vogt 2020). This unfortunately lies outside the scope of our paper.

We wish to conclude with a general assessment of the application of supervised ML in general and the GBDT al-

gorithm in particular to cosmological problems and to the estimation of the parameters of given cosmological objects like the LG. The analysis presented here has been formulated within a clear framework: a. The standard cosmological model (Λ CDM) is assumed; b. A LG model, which defines what a mock LG is; c. Observational uncertainties of the input parameters are assumed to be normally distributed. The GBDT algorithm is constructed as a multi-parameter non-linear fitting procedure, whose parameters are fixed by following the prior assumptions (Λ CDM and the LG model). The algorithm is then applied to the ensemble of the Monte Carlo realization of the input observational data and its uncertainties, thereby it constitutes a non-linear mapping from the prior probability distribution function of the input data to the posterior distribution functions of the predicted parameters. It follows that the GBDT algorithm in particular and supervised ML tools constitute a framework that is similar in its nature to the Bayesian approach, as all the conclusions and results presented here are strictly valid only under the assumptions of the Λ CDM and the LG models and given the observed values of the distance and relative velocity of the MW and M31 galaxies.

ADDENDUM

After the submission of the paper we came across the work of Villanueva-Domingo et al. (2021) who have estimated the masses of the MW and M31 galaxies by means of an ML technique, the graph neural networks, from a set of hydrodynamic cosmological simulations. In that study the issue of whether the MW and M31 galaxies are members of the LG is not considered. The resulting estimated mass of the M31 of that study is in very good agreement with ours. As for the MW galaxy, Villanueva-Domingo et al. (2021) have two different ways of estimating the mass, with and without including the velocities of satellites of the studied galaxies in their input data. The MW mass of the 'without the velocities' case is in a very good agreement with our estimation while in the other case the estimations are more than 1 sigma apart. In all cases the error bars presented here are smaller by roughly a factor of 2 or larger than those of Villanueva-Domingo et al. (2021).

ACKNOWLEDGEMENTS

This work has been done within the framework of the Constrained Local Universe Simulations (CLUES) simulations. YH has been partially supported by the Israel Science Foundation grant ISF 1358/18. NIL acknowledges financial support of the Project IDEXLYON at the University of Lyon under the Investments for the Future Program (ANR-16-IDEX-0005).

DATA AVAILABILITY

The code used for the GBDT, the analysis and the plots is freely available on the lead author's GitHub repository: <https://github.com/EdoardoCarlesi/MLEKO>. The simulation data used for the training of the GBDT algorithm

can be obtained by contacting the lead author at ecarlesi83@gmail.com.

REFERENCES

- Baiesi Pillastrini G. C., 2009, MNRAS, 397, 1990
 Battaglia G., Helmi A., Morrison H., Harding P., Olszewski E. W., Mateo M., Freeman K. C., Norris J., Shectman S. A., 2005, Mon. Not. Roy. Astron. Soc., 364, 433
 Boylan-Kolchin M., Bullock J. S., Kaplinghat M., 2012, MNRAS, 422, 1203
 Boylan-Kolchin M., Bullock J. S., Sohn S. T., Besla G., van der Marel R. P., 2013, ApJ, 768, 140
 Carlesi E., Hoffman Y., Gottlöber S., Libeskind N. I., Knebe A., Yepes G., Pilipenko S. V., 2019, MNRAS
 Carlesi E., Hoffman Y., Sorce J. G., Gottlöber S., 2017, MNRAS, 465, 4886
 Carlesi E., Hoffman Y., Sorce J. G., Gottlöber S., Yepes G., Courtois H., Tully R. B., 2016, MNRAS, 460, L5
 Carlesi E., Mota D. F., Winther H. A., 2017, MNRAS, 466, 4813
 Collister A. A., Lahav O., 2004, PASP, 116, 345
 Diaz J. D., Kopolov S. E., Irwin M., Belokurov V., Evans N. W., 2014, MNRAS, 443, 1688
 Elahi P. J., Lewis G. F., Power C., Carlesi E., Knebe A., 2015, MNRAS, 452, 1341
 Fardal M. A., et al., 2013, MNRAS, 434, 2779
 Fattahi A., Navarro J. F., Sawala T., Frenk C. S., Oman K. A., Crain R. A., Furlong M., Schaller M., Schaye J., Theuns T., Jenkins A., 2016, MNRAS, 457, 844
 Fragione G., Loeb A., 2017, NewA, 55, 32
 Freund Y., Schapire R. E., 1997, Journal of Computer and System Sciences, 55, 119
 Friedman J. H., 2001, The Annals of Statistics, 29, 1189
 Gaia Collaboration 2016, A&A, 595, A1
 Garaldi E., Baldi M., Moscardini L., 2016, JCAP, 1, 050
 Gibbons S. L. J., Belokurov V., Evans N. W., 2014, MNRAS, 445, 3788
 González R. E., Kravtsov A. V., Gnedin N. Y., 2014, ApJ, 793, 91
 Gottesman S. T., Hunter J. H., Boonyasait V., 2002, MNRAS, 337, 34
 Ibata R., Chapman S., Ferguson A. M. N., Irwin M., Lewis G., McConnachie A., 2004, MNRAS, 351, 117
 Kahn F. D., Woltjer L., 1959, ApJ, 130, 705
 Karachentsev I. D., Kashibadze O. G., Makarov D. I., Tully R. B., 2009, MNRAS, 393, 1265
 Knollmann S. R., Knebe A., 2009, ApJS, 182, 608
 Lemos P., Jeffrey N., Whiteway L., Lahav O., Libeskind N., Hoffman Y., 2021, Phys. Rev. D, 103, 023009
 Linardatos P., Papastefanopoulos V., Kotsiantis S., 2021, Entropy, 23
 Lucie-Smith L., Peiris H. V., Pontzen A., 2019, MNRAS, 490, 331
 Lucie-Smith L., Peiris H. V., Pontzen A., Lochner M., 2018, MNRAS, 479, 3405
 Lucie-Smith L., Peiris H. V., Pontzen A., Nord B., Thiya-galingam J., 2020, arXiv e-prints, p. arXiv:2011.10577
 Lynden-Bell D., 1981, The Observatory, 101, 111
 Machado Poletti Valle L. F., Avestruz C., Barnes D. J.,

- Farahi A., Lau E. T., Nagai D., 2020, arXiv e-prints, p. arXiv:2011.12987
- Marcinkevičs R., Vogt J. E., 2020, arXiv e-prints, p. arXiv:2012.01805
- McLeod M., Lahav O., 2020, JCAP, 2020, 056
- McLeod M., Libeskind N., Lahav O., Hoffman Y., 2017, JCAP, 2017, 034
- McMillan P. J., 2011, MNRAS, 414, 2446
- McMillan P. J., 2016, ArXiv e-prints
- Merten J., Giocoli C., Baldi M., Meneghetti M., Peel A., Lalande F., Starck J.-L., Pettorino V., 2019, MNRAS, 487, 104
- Mucesh S., et al., 2021, MNRAS
- Naim A., Lahav O., Sodre L. J., Storrie-Lombardi M. C., 1995, MNRAS, 275, 567
- Partridge C., Lahav O., Hoffman Y., 2013, MNRAS, 436, L45
- Peñarrubia J., Gómez F. A., Besla G., Erkal D., Ma Y.-Z., 2016, MNRAS, 456, L54
- Pedregosa F., Varoquaux G., Gramfort A., Michel V., Thirion B., Grisel O., Blondel M., Prettenhofer P., Weiss R., Dubourg V., Vanderplas J., Passos A., Cournapeau D., Brucher M., Perrot M., Duchesnay E., 2011, Journal of Machine Learning Research, 12, 2825
- Peel A., Lalande F., Starck J.-L., Pettorino V., Merten J., Giocoli C., Meneghetti M., Baldi M., 2019, Phys. Rev. D, 100, 023508
- Penzo C., Macciò A. V., Baldi M., Casarini L., Oñorbe J., Dutton A. A., 2016, MNRAS, 461, 2490
- Planck Collaboration 2014, A&A, 571, A16
- Press W. H., Teukolsky S. A., Vetterling W. T., Flannery B. P., 2002, Numerical recipes in C++ : the art of scientific computing
- Tollerud E. J., Boylan-Kolchin M., Bullock J. S., 2014, MNRAS, 440, 3511
- van der Marel R. P., Fardal M., Besla G., Beaton R. L., Sohn S. T., Anderson J., Brown T., Guhathakurta P., 2012, ApJ, 753, 8
- van der Marel R. P., Fardal M. A., Sohn S. T., Patel E., Besla G., del Pino A., Sahlmann J., Watkins L. L., 2019, ApJ, 872, 24
- Villanueva-Domingo P., Villaescusa-Navarro F., Genel S., Anglés-Alcázar D., Hernquist L., Marinacci F., Spergel D. N., Vogelsberger M., Narayanan D., 2021, arXiv e-prints, p. arXiv:2111.14874
- Watkins L. L., van der Marel R. P., Sohn S. T., Evans N. W., 2019, ApJ, 873, 118
- Zavala J., Avila-Reese V., Firmani C., Boylan-Kolchin M., 2012, MNRAS, 427, 1503

This paper has been typeset from a \TeX / \LaTeX file prepared by the author.